Electronic Supporting Information for: First principles investigation of manganese catalyst structure and coordination in the p-xylene oxidation process

Harry N. Thomas [1], Duncan Wass [1], Caroline A. Offiler [2], Keith Whiston [2], Andrew J. Logsdail [1]

Corresponding author: LogsdailA@cardiff.ac.uk

[1] *Cardiff Catalysis Institute, School of Chemistry, Park Place, Cardiff University, Cardiff, CF10 3AT, United Kingdom.*

[2] *Koch Technology Solutions Ltd., The Wilton Centre, Wilton, Redcar, TS10 4RE.*

S1 Benchmarking of parameters for first principles calculations

A variety of density functionals were tested to identify the most appropriate settings to accurately determine the structural properties of the manganese catalyst. The ability of the density functionals to predict the structural properties was assessed by calculating the Mn – O bond lengths for Mn(II) hexahydrate, and benchmarking against the experimental values.[1,2] The density functionals tested include PBE, PBE0 and M06, and the results are shown in Table S1. For the presented density functionals, the Mn–O bond length was predicted to be within 0.04 Å of the experimental value. The hybrid density functionals (PBE0, M06) marginally predict the upper bounds of the Mn–O bond lengths better, with M06 providing the best estimate; however, the time taken per self-consistent field (SCF) cycle for each of the PBE, PBE0 and M06 functionals were 0.60 seconds, 7.44 seconds and 8.29 seconds, respectively.[3–5] The computational cost of the hybrid density functionals to evaluate the SCF cycle, relative to the small increase in accuracy, meant PBE was chosen for the geometry optimisations.

Table S1 Mn–O bond lengths (Å) for $[Mn(H_2O)_6]^{2+}$ calculated with the PBE, PBE0, and M06 exchange correlation density functionals. An experimental reference value is also provided.[1,2] Calculations were performed using a "tight" basis, a high-spin configuration, and with no dispersion correction.

PBE	PBE0	M06	Experiment
2.18-2.24	2.18-2.23	2.16-2.20	2.17-2.20

The impact of the default basis sets in FHI-Aims on the predicted Mn–O bond lengths were also evaluated, with the results shown in Table S2. The bond lengths are marginally reduced (0.01 Å) when increasing the basis completeness from 'light' to 'tight'; the inclusion of additional basis functions (i.e., 'really tight') provides no further accuracy gains. An 'intermediate' basis exists for light elements, but was not considered further as manganese was unavailable. The time taken per SCF cycle is 0.14, 0.60, and 9.66 seconds, for the 'light', 'tight' and 'really tight' basis sets, respectively. The fourfold increase in time per SCF cycle between 'light' and 'tight' basis settings remains computationally tractable, and the greater accuracy rewarded meant that the 'tight' basis was chosen for geometry optimisations.

Table S2 Mn–O bond lengths (Å) for $[Mn(H_2O)_6]^{2+}$ calculated with the distributed basis sets in FHI-aims.[6] An experimental reference value is also provided.[1,2] Calculations were performed using the PBE density functional, a high-spin configuration, and with no dispersion correction.

'light'	'tight'	'really tight'	Experiment
2.19 - 2.25	2.18 - 2.24	2.18 - 2.24	2.17 - 2.20

Due to the importance of inter-molecular interactions in our systems, a dispersion correction was tested. The Tkatchenko-Scheffler method and non-local many body dispersion (MBD) were considered, with the results shown in Table S3.[7–9] The non-local MBD scheme gave a marginally more accurate upper-bound on the bond lengths, by 0.01 Å, whilst the Tkatchenko-Scheffler method results in no change in Mn–O bond lengths. Given that the non-local MBD approach provides enhanced structural properties for a trivial increase in computational time, this scheme was used for subsequent geometry optimisations.

Table S3 Mn–O bond lengths (Å) for $[Mn(H_2O)_6]^{2+}$ calculated with no vdW correction, a long-range vdW correction (Tkatchenko-Scheffler method, TS) and the non-local MBD correction. An experimental reference value is also provided.[1,2] Calculations were performed using the PBE density functional, a "tight" basis, and a high-spin configuration.

None	Tkatchenko-Scheffler	MBD	Experiment
2.18 - 2.24	2.18 - 2.24	2.18 - 2.23	2.17 - 2.20

S2 Parametrisation of MPB electrostatic parameters

The long-range dielectric response of the solvent environment was accounted for by running single-point implicit solvation calculations on the gas-phase optimized complexes using the size-modified Poisson Boltzmann (MPB) scheme. The electrostatic parameters ($\rho_{\min}$, $\rho_{\max}$) for the MPB scheme were parameterised for implicit water and acetic acid separately. The parameterisation was done by performing DFT calculations over a two dimensional $\{\rho_{\min}, \rho_{\max}\}$ grid for water and acetic acid, with dielectric constants of 78.358 and 6.2528, respectively, and the obtained Free Energy of solvation was benchmarked against the experimental Free Energies of solvation for the solute in the solvent, as obtained from the Minnesota Solvation Database. [10,11] Plots of the mean signed errors (MSE) of the Free Energy of solvation, obtained using the PBE0 density functional, are presented relative to experimental references from the Minnesota solvation database. [10,11] These plots are shown in Figure S1. Any combination of $\{\rho_{\min}, \rho_{\max}\}$ where the MSE contour line is zero may be deemed adequate choices for the electrostatic parameters; for implicit water, the isodensity cavity cutoffs of $\rho_{\min}$=0.00025 e and $\rho_{\max}$=0.003 e were chosen, and for implicit acetic acid, parameters of $\rho_{\min}$=0.00025 e, $\rho_{\max}$=0.002 e were chosen.

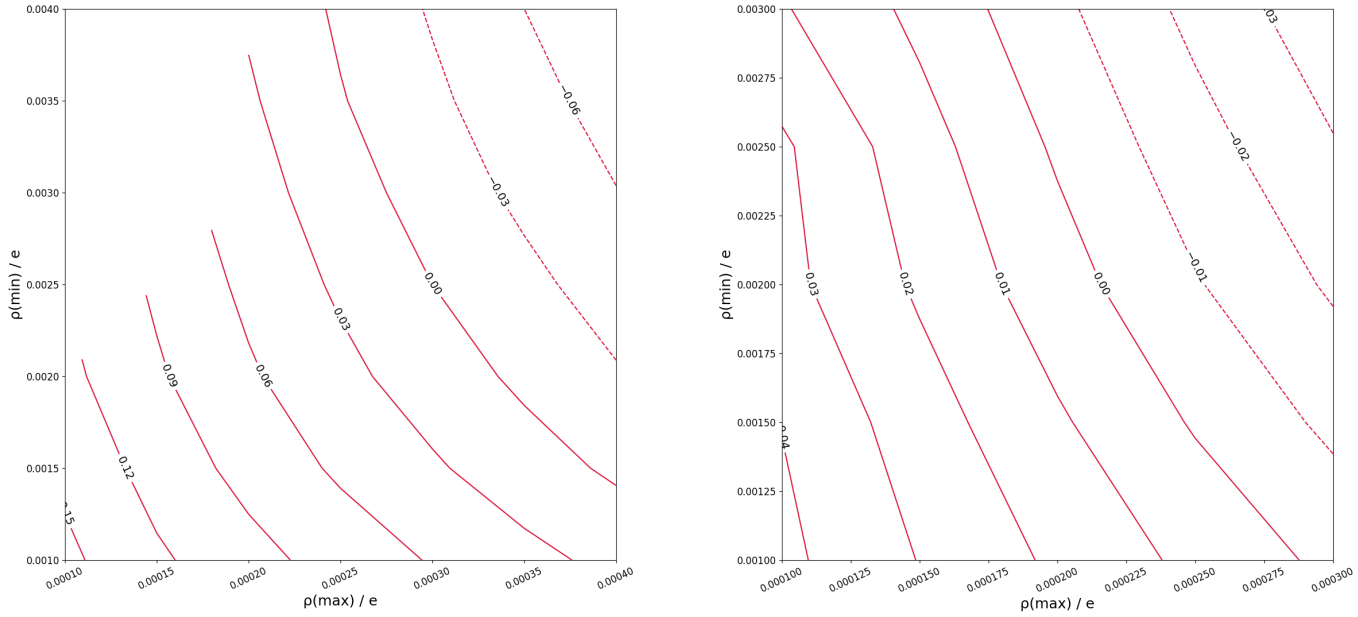

Fig. S1 Contour plots of the isodensity cutoffs, $\rho_{\min}$ and $\rho_{\max}$, plotted against the MSE of the SCCS free solvation energy relative to an experimental reference from the Minnesota Solvation database. [10,11] Left: water; Right: trans isomer of acetic acid.

The optimal values of $\{\rho_{\min}, \rho_{\max}\}$ are observed to have a dependence on the density functional applied to evaluate the exchange-correlation energy. The values reported above, and used in the main text, were obtained using PBE0 density functional.

S3 Structural and energetics data associated with the molecular DFT calculations

S3.1 Mn(II) and Mn(III) complexes

To determine the relative Gibbs Free Energies of different inner-sphere coordinated ligands for Mn(II) and Mn(III), all symmetry inequivalent geometric isomers were considered for geometry optimisations (Figures S2–S10), where the geometric isomers are labelled numerically. The geometric isomers with the lowest solvation-phase Free Energy, for any given combination of ligands, were used further in evaluating the energies for ligand substitution.

In order to ensure validity of the isomer energies when evaluating structure choices, isomers were only considered as valid when the structure coordination did not change during optimisation; systems were not considered further in our evaluations when changes occurred in metal cation coordination number, such as dissociation of water and acetic acid ligands or changes in coordination mode of acetate ligands. In addition, self-consistent field cycle convergence was deemed infeasible for few select complexes, which meant Free Energies could not be evaluated. Structures for which Free Energies were not able to be determined includes: $Mn(OAc)_2(H_2O)_3$, $Mn(OAc)_2(H_2O)_2$ and $Mn(OAc)_2(HOAc)_1(H_2O)_1$.

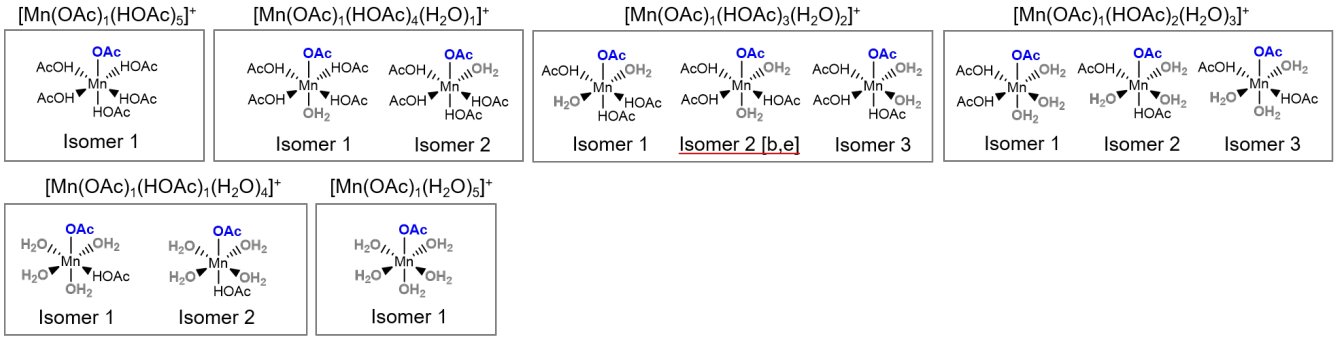

Fig. S2 Figure of the considered geometric isomers for the (+1) charged Mn(II) complex with one monodentate acetate, as a function of water and acetic acid ligands. Isomers underlined in red were not considered, due to either changes in structure coordination upon optimization. The changes in structure considered include: a) deprotonation of water; b) change in acetate coordination; c) dissocation of acetic acid; d) dissociation of water; e) change to seven coordinate species; f) change to five coordinate species; g) change to four coordinate species; h) interconverts to a different isomer.

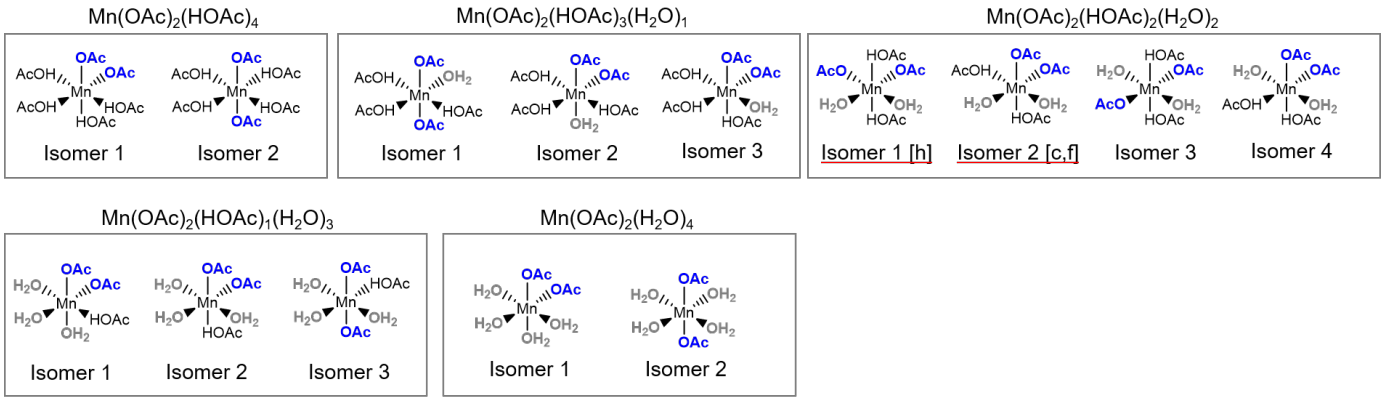

Fig. S3 Figure of the considered geometric isomers for the neutrally charged Mn(II) complex with two monodentate acetate, as a function of water and acetic acid ligands. Isomers underlined in red were not considered, due to either changes in structure coordination upon optimization. Changes in structure include [a] deprotonation of water, [b] change in acetate coordination, [c] dissocation of acetic acid, [d] dissociation of water, [e] change to seven coordinate species, [f] change to five coordinate species, [g] change to four coordinate species, [h] converts to a different isomer.

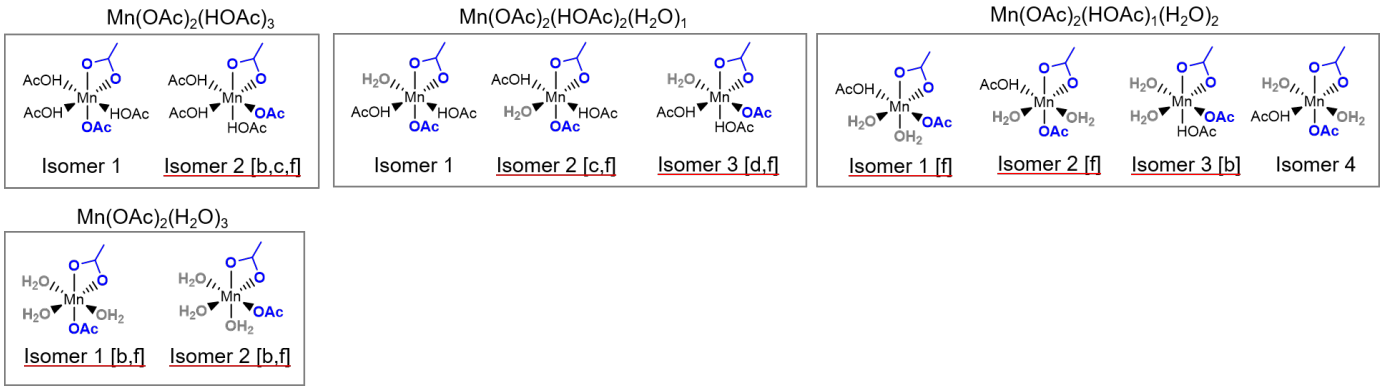

Fig. S4 Figure of the considered geometric isomers for the neutrally charged Mn(II) complex with one monodentate acetate and one chelating bidentate acetate ligand, as a function of water and acetic acid ligands. Isomers underlined in red were not considered, due to either changes in structure coordination upon optimization. Changes in structure include [a] deprotonation of water, [b] change in acetate coordination, [c] dissocation of acetic acid, [d] dissociation of water, [e] change to seven coordinate species, [f] change to five coordinate species, [g] change to four coordinate species, [h] converts to a different isomer.

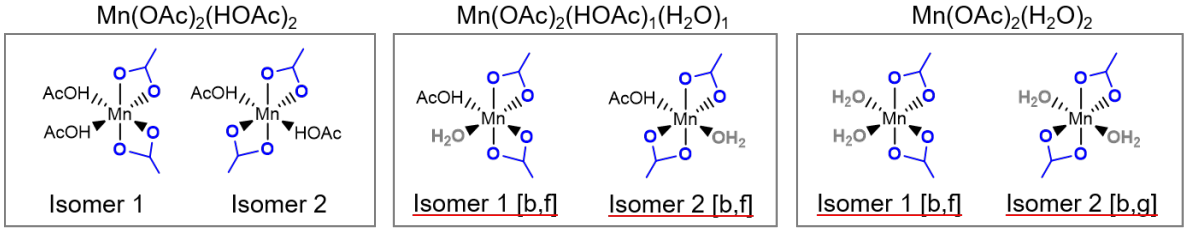

Fig. S5 Figure of the considered geometric isomers for the neutrally charged Mn(II) complex with two chelating bidentate acetate ligand, as a function of water and acetic acid ligands. Isomers underlined in red were not considered, due to either changes in structure coordination upon optimization. Changes in structure include [a] deprotonation of water, [b] change in acetate coordination, [c] dissocation of acetic acid, [d] dissociation of water, [e] change to seven coordinate species, [f] change to five coordinate species, [g] change to four coordinate species, [h] converts to a different isomer.

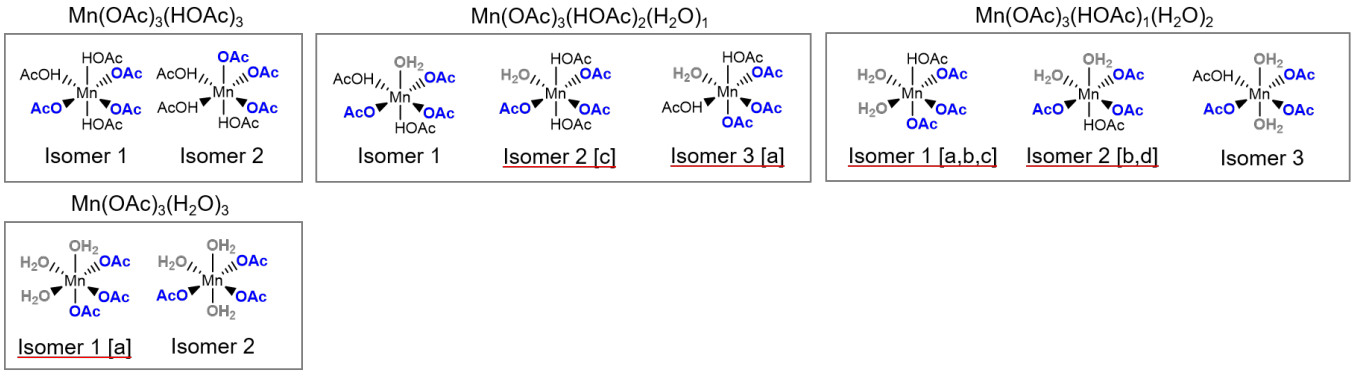

Fig. S6 Figure of the considered geometric isomers for the neutrally charged Mn(III) complex with three monodentate acetate ligand, as a function of water and acetic acid ligands. Isomers underlined in red were not considered, due to either changes in structure coordination upon optimization. Changes in structure include [a] deprotonation of water, [b] change in acetate coordination, [c] dissocation of acetic acid, [d] dissociation of water, [e] change to seven coordinate species, [f] change to five coordinate species, [g] change to four coordinate species, [h] converts to a different isomer.

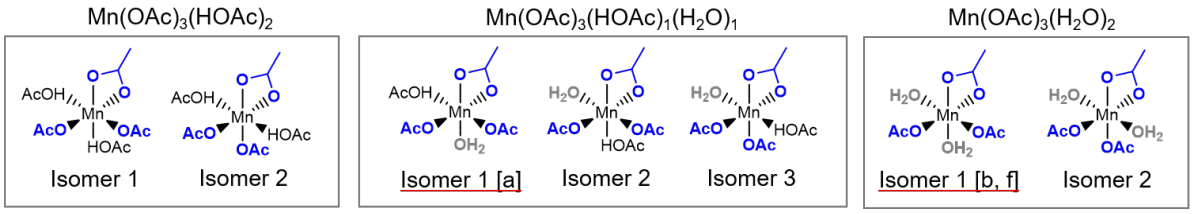

Fig. S7 Figure of the considered geometric isomers for the neutrally charged Mn(III) complex with two monodentate acetate ligand and one chelating bidentate acetate ligand, as a function of water and acetic acid ligands. Isomers underlined in red were not considered, due to either changes in structure coordination upon optimization. Changes in structure include [a] deprotonation of water, [b] change in acetate coordination, [c] dissocation of acetic acid, [d] dissociation of water, [e] change to seven coordinate species, [f] change to five coordinate species, [g] change to four coordinate species, [h] converts to a different isomer.

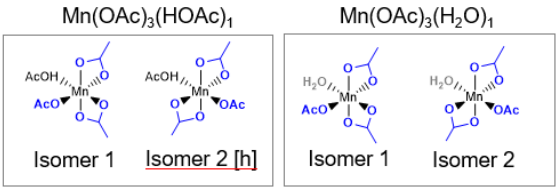

Fig. S8 Figure of the considered geometric isomers for the neutrally charged Mn(III) complex with one monodentate acetate ligand and two chelating bidentate acetate ligand, as a function of water and acetic acid ligands. Isomers underlined in red were not considered, due to either changes in structure coordination upon optimization. Changes in structure include [a] deprotonation of water, [b] change in acetate coordination, [c] dissocation of acetic acid, [d] dissociation of water, [e] change to seven coordinate species, [f] change to five coordinate species, [g] change to four coordinate species, [h] converts to a different isomer.

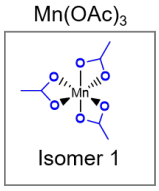

Fig. S9 Figure of the considered geometric isomers for the neutrally charged Mn(III) complex with three chelating bidentate acetate ligand, as a function of water and acetic acid ligands. Isomers underlined in red were not considered, due to either changes in structure coordination upon optimization. Changes in structure include [a] deprotonation of water, [b] change in acetate coordination, [c] dissocation of acetic acid, [d] dissociation of water, [e] change to seven coordinate species, [f] change to five coordinate species, [g] change to four coordinate species, [h] converts to a different isomer.

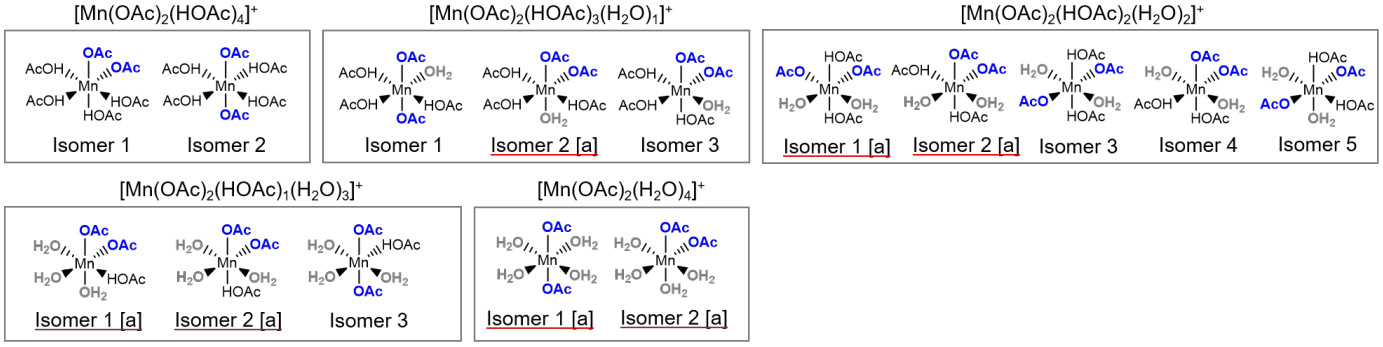

Fig. S10 Figure of the considered geometric isomers for the (+1) charged Mn(III) complex with two monodentate acetate ligand, as a function of water and acetic acid ligands. Isomers underlined in red were not considered, due to either changes in structure coordination upon optimization. Changes in structure include [a] deprotonation of water, [b] change in acetate coordination, [c] dissocation of acetic acid, [d] dissociation of water, [e] change to seven coordinate species, [f] change to five coordinate species, [g] change to four coordinate species, [h] converts to a different isomer.

The $E_{\mathrm{ZPE}} + pV$, the entropy (TS), the solvated electronic energy (E_{solv}), and the solvated Gibbs Free Energy (G_{solv}) for the most stable geometric isomer are shown in Tables S4–S12. The 'isomer' column shows which of the considered geometric isomers (see Figures S2–S10) were the most stable (had the lowest G_{solv}). Note that the G_{solv} values shown are calculated using

$$G_{\mathrm{solv}} = E_{\mathrm{solv}} + (E_{\mathrm{ZPE}} + pV) - TS \tag{1}$$

which is an equivalent expression to equation 3 shown in the methodgy. G_{solv} are obtained within the ideal gas limit at T = 473 K, p = 2.25 MPa, unless stated otherwise.

Table S4 Enthalpy, entropy and solvated energy for the geometric isomers with the lowest Free Energies, considering a (+1) charged Mn(II) complex with one monodentate acetate ligands as a function of the coordinating water and acetic acid ligands. Values are given in units of eV.

Ligand environment	Isomer	$E_{\mathrm{ZPE}} + pV$	TS	E_{solv}	G_{solv}
1 acetate, 0 water, 5 acetic acid	1	11.770	6.589	-69038.954	-69033.773
1 acetate, 1 water, 4 acetic acid	2	10.537	5.997	-64884.118	-64879.578
1 acetate, 2 water, 3 acetic acid	3	9.335	5.461	-60729.122	-60725.248
1 acetate, 3 water, 2 acetic acid	2	8.167	4.897	-56574.405	-56571.135
1 acetate, 4 water, 1 acetic acid	2	6.936	4.561	-52419.293	-52416.918
1 acetate, 5 water, 0 acetic acid	1	5.773	3.702	-48264.328	-48262.257

Table S5 Enthalpy, entropy and solvated energy for the geometric isomers with the lowest Free Energies, considering an octahedrally coordinated Mn(II) complex with two monodentate acetate ligands as a function of the coordinating water and acetic acid ligands. Values are given in units of eV.

Ligand environment	Isomer	$E_{\mathrm{ZPE}} + pV$	TS	E_{solv}	G_{solv}
2 acetate, 0 water, 4 acetic acid	1	11.383	6.406	-69026.531	-69021.554
2 acetate, 1 water, 3 acetic acid	3	10.172	6.019	-64871.840	-64867.687
2 acetate, 2 water, 2 acetic acid	4	8.995	5.133	-60717.173	-60713.311
2 acetate, 3 water, 1 acetic acid	1	7.778	4.669	-56562.472	-56559.363
2 acetate, 4 water, 0 acetic acid	2	6.598	4.235	-52407.518	-52405.155

Table S6 Enthalpy, entropy and solvated energy for the geometric isomers with the lowest Free Energies, considering a Mn(II) complex with one chelating and one monodentate acetate ligands as a function of the coordinating water and acetic acid ligands. Values are given in units of eV. NA indicates a ligand configuration is not applicable for the given metal cation coordination.

Ligand environment	Isomer	$E_{\mathrm{ZPE}} + pV$	TS	E_{solv}	G_{solv}
2 acetate, 0 water, 3 acetic acid	1	9.386	5.536	-62790.550	-62786.700
2 acetate, 1 water, 2 acetic acid	1	8.17	4.985	-58635.955	-58632.770
2 acetate, 2 water, 1 acetic acid	4	6.989	4.476	-54480.715	-54478.202
2 acetate, 3 water, 0 acetic acid	NA	NA	NA	NA	NA

Table S7 Enthalpy, entropy and solvated energy for the geometric isomers with the lowest Free Energies, considering a Mn(II) complex with two chelating acetate ligands as a function of the coordinating water and acetic acid ligands. Values are given in units of eV. NA indicates a ligand configuration is not applicable for the given metal cation coordination.

Ligand environment	Isomer	$E_{\mathrm{ZPE}} + pV$	TS	E_{solv}	G_{solv}
2 acetate, 0 water, 2 acetic acid	1	7.384	4.848	-56554.360	-56551.824
2 acetate, 1 water, 1 acetic acid	NA	NA	NA	NA	NA
2 acetate, 2 water, 0 acetic acid	NA	NA	NA	NA	NA

Table S8 Enthalpy, entropy and solvated energy for the geometric isomers with the lowest Free Energies, considering a (+1) charged Mn(III) complex with two monodentate acetate ligands as a function of the coordinating water and acetic acid ligands. Values are given in units of eV. NA indicates a ligand configuration is not applicable for the given metal cation coordination.

Ligand environment	Isomer	$E_{\mathrm{ZPE}} + pV$	TS	E_{solv}	G_{solv}
2 acetate, 0 water, 4 acetic acid	1	11.425	5.983	-69021.898	-69016.456
2 acetate, 1 water, 3 acetic acid	1	10.170	5.497	-64867.367	-64862.695
2 acetate, 2 water, 2 acetic acid	3	8.921	4.926	-60712.488	-60708.493
2 acetate, 3 water, 1 acetic acid	3	7.723	4.444	-56557.393	-56554.114
2 acetate, 4 water, 0 acetic acid	NA	NA	NA	NA	NA

Table S9 Enthalpy, entropy and solvated energy for the geometric isomers with the lowest Free Energies, considering a Mn(III) complex with three monodentate acetate ligands as a function of the coordinating water and acetic acid ligands. Values are given in units of eV.

Ligand environment	Isomer	$E_{\mathrm{ZPE}} + pV$	TS	E_{solv}	G_{solv}
3 acetate, 0 water, 3 acetic acid	1	11.057	6.141	-69009.998	-69005.082
3 acetate, 1 water, 2 acetic acid	1	9.848	5.439	-64855.300	-64850.891
3 acetate, 2 water, 1 acetic acid	3	8.654	4.884	-60700.063	-60696.293
3 acetate, 3 water, 0 acetic acid	2	7.407	4.365	-56545.531	-56542.489

Table S10 Enthalpy, entropy and solvated energy for the geometric isomers with the lowest Free Energies, considering a Mn(III) complex with one chelating and two monodentate acetate ligands as a function of the coordinating water and acetic acid ligands. Values are given in units of eV.

Ligand environment	Isomer	$E_{\mathrm{ZPE}} + pV$	TS	E_{solv}	G_{solv}
3 acetate, 0 water, 2 acetic acid	1	9.049	5.091	-62773.686	-62769.728
3 acetate, 1 water, 1 acetic acid	3	7.840	4.762	-58619.120	-58616.042
3 acetate, 2 water, 0 acetic acid	2	6.639	4.102	-54464.405	-54461.868

Table S11 Enthalpy, entropy and solvated energy for the geometric isomers with the lowest Free Energies, considering a Mn(III) complex with two chelating and one monodenate acetate ligands as a function of the coordinating water and acetic acid ligands. Values are given in units of eV.

Ligand environment	Isomer	$E_{\mathrm{ZPE}} + pV$	TS	E_{solv}	G_{solv}
3 acetate, 0 water, 1 acetic acid	1	7.045	4.199	-56537.640	-56534.794
3 acetate, 0 water, 1 acetic acid	2	5.782	3.900	-52382.895	-52381.013

Table S12 Enthalpy, entropy and solvated energy for the geometric isomers with the lowest Free Energies, considering a Mn(III) complex with three chelating acetate ligands as a function of the coordinating water and acetic acid ligands. Values are given in units of eV.

Ligand environment	Isomer	$E_{\mathrm{ZPE}} + pV$	TS	E_{solv}	G_{solv}
3 acetate, 0 water, 0 acetic acid	1	5.032	3.655	-50301.056	-50299.679

S3.2 Ligands

This section shows the energetic properties for the considered ligands; water, acetic acid (cis conformer), and acetate.

Table S13 Enthalpy, entropy, and solvated energy for the considered ligands. Values are given in units of eV.

Ligand environment	$E_{\mathrm{ZPE}} + pV$	TS	E_{solv}	G_{solv}
H_2O	0.730	0.905	-2081.142	-2081.317
CH_3COOH	1.925	1.475	-6236.118	-6235.668
CH_3COO^-	1.547	1.527	-6223.039	-6223.019

S4 Assessment of the effect of temperature and pressure on the Free Energy landscape

The effect of the temperature and pressure on the Gibbs Free Energy was investigated for the most stable Mn(II) complexes, to explore how the catalyst structures might vary under different operating conditions. Figures S11 – S13 show the Free Energy landscapes at three different temperatures and pressures: (i) industrial operating conditions (T = 473 K, p = 2.25 MPa); (ii) standard conditions (T = 298 K, p = 0.1 MPa); and (iii) the conditions at which the ESEEM measurements by Taylor *et al.* were obtained (T = 5 K, p = 0.1 MPa).[12] There is no qualitative difference in the results when comparing industrial and standard conditions, with $Mn(OAc)_2(HOAc)_2$ the most energetically preferable structure. Reduction of the temperature from 298 K to 5 K, as per Figure S13, is found to disfavour acetate chelation, with $Mn(OAc)_2(H_2O)_3(HOAc)_1$ found to be the most energetically preferable complex.

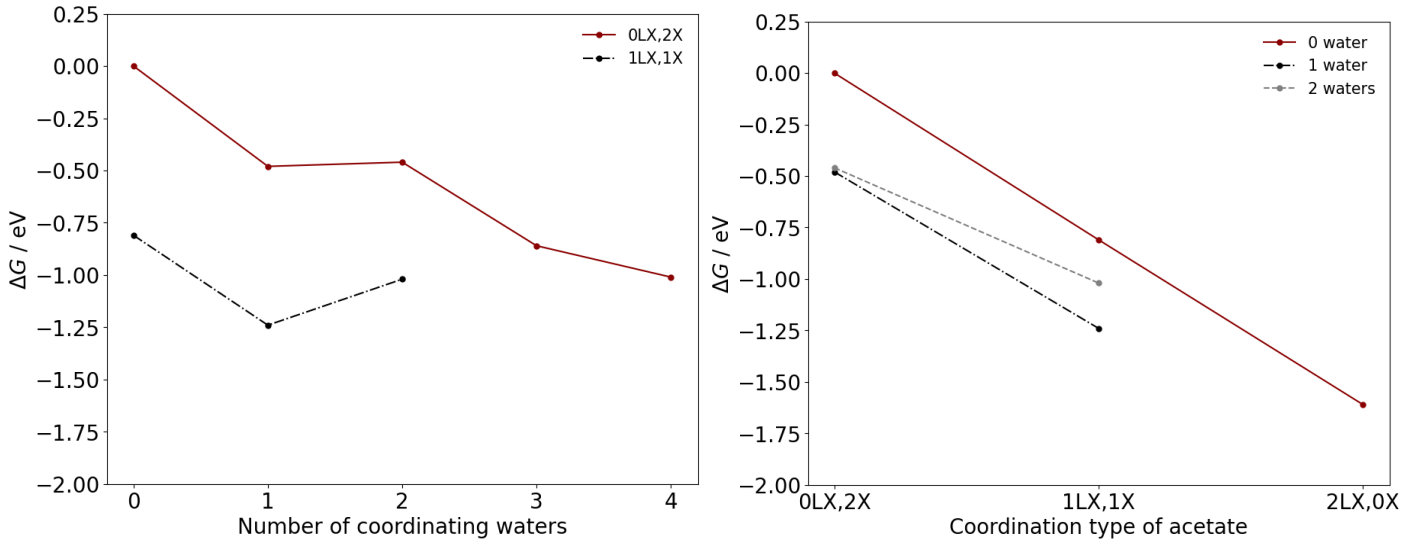

Fig. S11 ΔG as calculated for octahedrally coordinated Mn(II) complexes for (left.) substitution of acetic acid for water and (right.) chelation of a coordinating monodentate acetate ligand. ΔG are calculated with the PBE0 density functional and include an implicit solvent model assuming a solvent environment of 34.6 mol% water in acetic acid, and a temperature and pressure of 473 K and 2.25 MPa, respectively. ΔG are calculated relative to the value of octahedrally coordinated $Mn(OAc)_2(HOAc)_4$, giving $\Delta G = 0$ for this species.

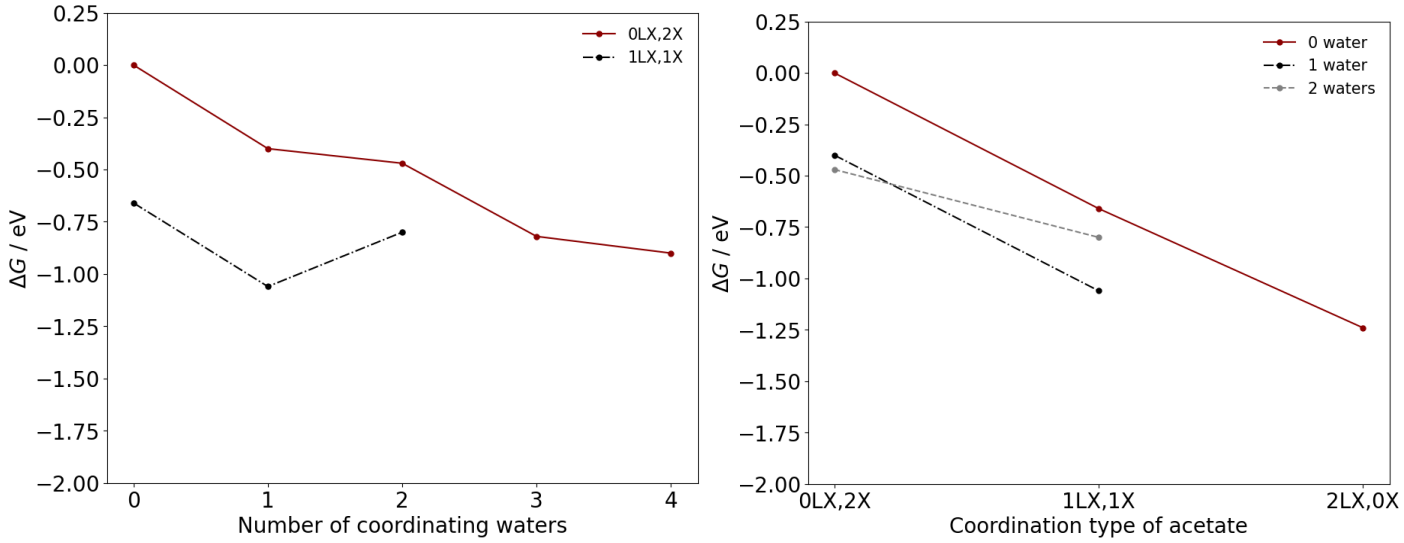

Fig. S12 ΔG as calculated for octahedrally coordinated Mn(II) complexes for (left) substitution of acetic acid for water and (right) chelation of a coordinating monodentate acetate ligand. ΔG are calculated with the PBE0 density functional and include an implicit solvent model assuming a solvent environment of 34.6 mol% water in acetic acid, and a temperature and pressure of 298 K and 0.1 MPa, respectively. ΔG are calculated relative to the value of octahedrally coordinated $\mathrm{Mn(OAc)_2(HOAc)_4}$, giving $\Delta G = 0$ for this species.

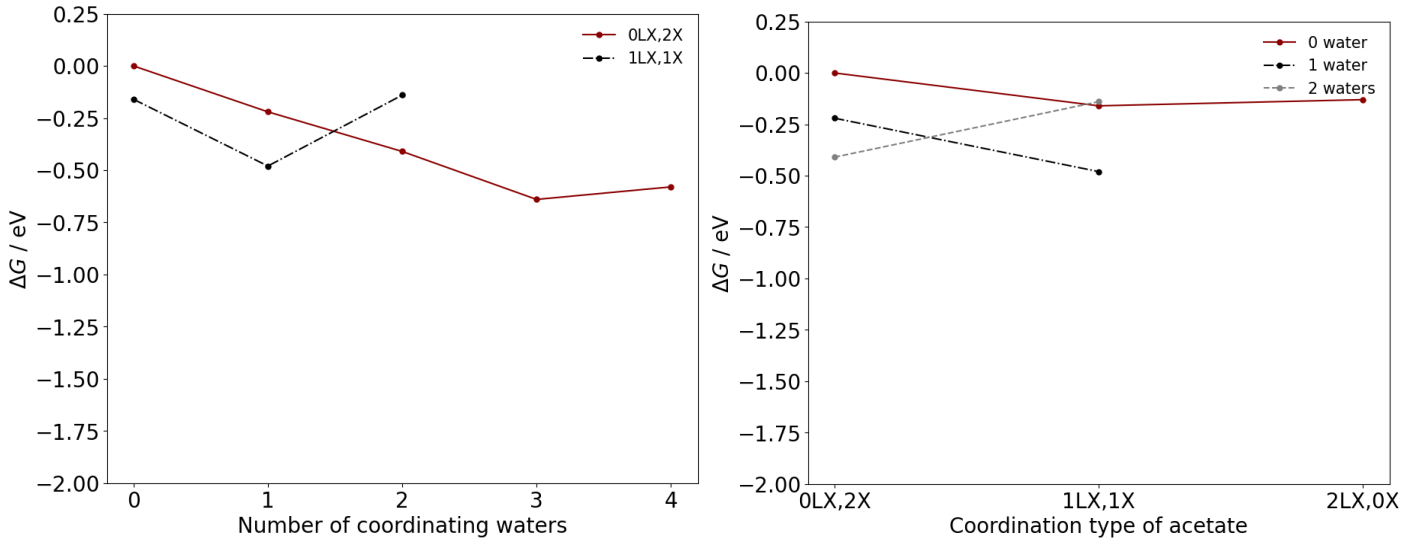

Fig. S13 ΔG as calculated for octahedrally coordinated Mn(II) complexes for (left) substitution of acetic acid for water and (right) chelation of a coordinating monodentate acetate ligand. ΔG are calculated with the PBE0 density functional and include an implicit solvent model assuming a solvent environment of 34.6 mol% water in acetic acid, and a temperature and pressure of 5 K and 0.1 MPa, respectively. ΔG are calculated relative to the value of octahedrally coordinated $\mathrm{Mn(OAc)_2(HOAc)_4}$, giving $\Delta G = 0$ for this species.

S5 Benchmarking of settings for the molecular dynamics simulations

S5.1 Reciprocal space sampling

Initially, a periodic model of the solvent system was created. A $3 \times 3 \times 3$ supercell was constructed from a unit cell containing one acetic acid, resulting in 27 solvent molecules. An initial density of 0.856 g/cm^3 was used, which corresponds to the experimental density of acetic acid at a temperature of 460 K and pressure of 1.55 MPa.[13] This density is for different operating conditions than the p-xylene oxidation commercial operating conditions (T = 473 K, p = 2.25 MPa), however is the closest available experimental density, and is just used for the purpose of benchmarking the MD settings. A **k**-grid is required to sample the reciprocal space under periodic boundary conditions, and thus calculations were performed for the acetic acid model with a Γ-centred $n \times n \times n$ **k**-mesh, with $1 \leq n \leq 6$. The rest of the calculation settings were the same as described in the molecular dynamics section of the methodology. Table S14 shows the system energy as a function of the **k**-grid density.

Table S14 Tabulated energies, force magnitudes and calculation length (maximum CPU time) as a function of the **k**-grid mesh dimensions for a $3 \times 3 \times 3$ super cell of acetic acid molecules.

k-grid	Energies / eV	Force magnitude / eV Å^{-1}	calculation length / s
1x1x1	-168365.581	0.004275	4622
2x2x2	-168365.718	0.004277	5313
3x3x3	-168365.722	0.004277	8387
4x4x4	-168365.722	0.004295	30011
5x5x5	-168365.722	0.004277	30176
6x6x6	-168365.722	0.004277	51965

The total energy changes by 5.2 meV/molecule when increasing n from 1 to 2, and by 0.1 meV/molecule when n increases to 3; above n = 3, the system energy is fully converged. The magnitude of forces on atoms was also evaluated, and the force is observed as less affected by a sparser **k**-grid, with n = 1 showing converged behaviour. As the objective of the molecular dynamics simulations was for accurate geometric representation of the solvated system in a tractable compute time, convergence of the forces was deemed the most important observable to determine simulation accuracy. Convergence of the atomic forces was observed at n = 1, and this provides an 45% compute efficiency gain compared to n = 3, which would provide accurate energetics.

S5.2 Calibration of timestep, and the thermostat coupling constant

The timestep for the integration algorithm used in the molecular dynamics simulations was parameterised. The benchmark molecular dynamics simulations were performed with a fixed number of moles, volume, and temperature (*i.e.*, an NVT ensemble). Simulations with timesteps of 1, 2, and 3 fs were tested for a duration of 500 fs; timesteps larger than 1 fs resulted in energetic instability, which meant 1 fs timestep was chosen for all further simulations.

To ensure the coupling constant between the simulation and the external heat bath was maintained accurately, a thermostat was calibrated for acetic acid at T = 460 K, p = 1.55 MPa, using the same settings as used for determining the **k**-grid. Figure S14 plots the system potential, kinetic, and total energy as a function of simulation time with varying coupling constant to the thermostat. Very short

coupling constants of 1 fs (not shown) resulted in energetic instability, which made them inappropriate, whilst the coupling constants of 400 and 800 fs resulted in very slow equilibration of the system. Test results showed that the coupling constants of 100 and 200 fs offered good balance and stability, with simulations extended to 1500 fs to confirm simulation stability. To allow maximum flexibility of the simulation cell, and represent the inhomogeneity of temperature changes under industrial operating conditions, the longer, weaker coupling constant of 200 fs was applied for dynamic simulations herein.

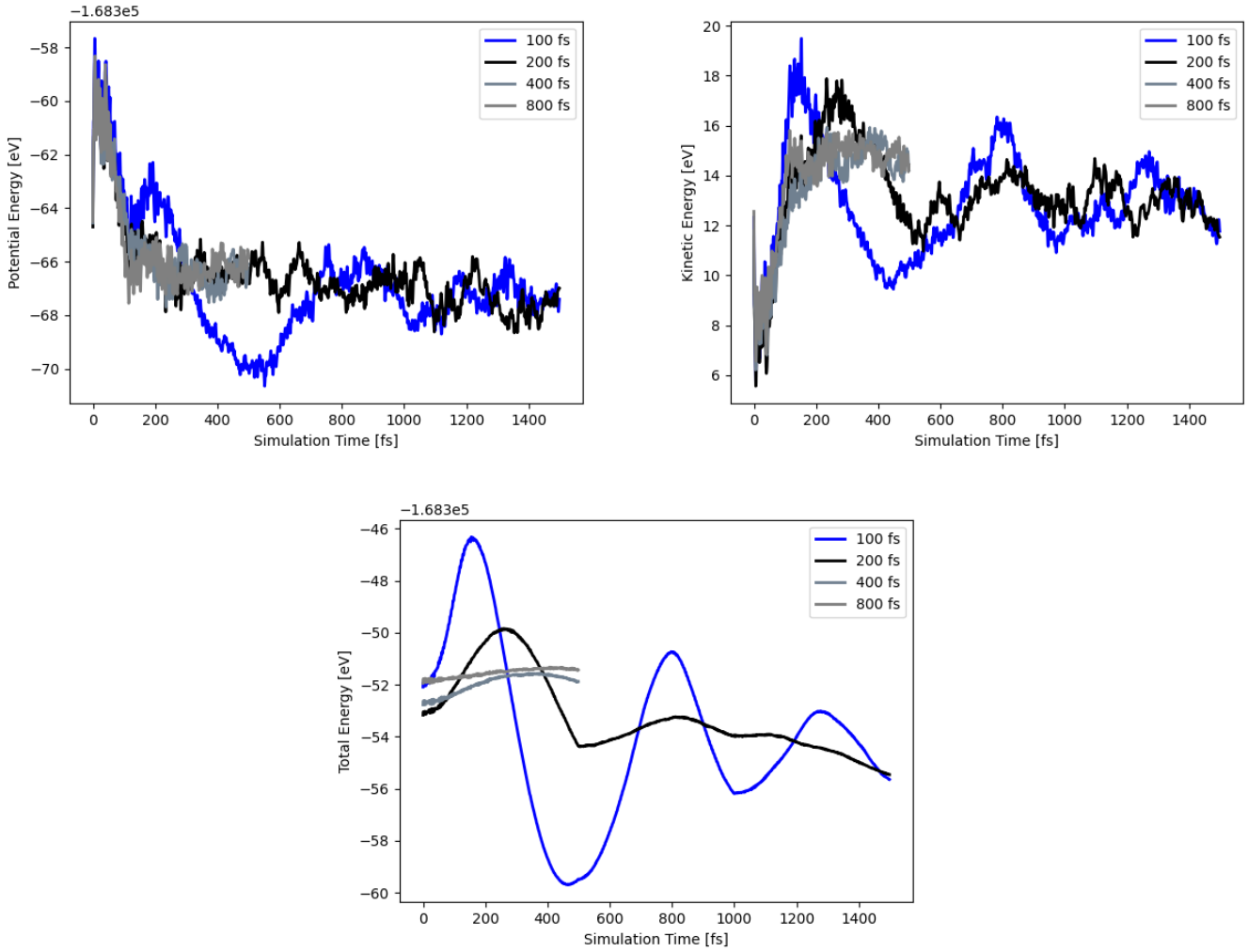

Fig. S14 Plots of the potential energy, kinetic energy, and total energy against simulation time for acetic acid at T = 460 K, p = 1.55 MPa. Various thermostat coupling constants were applied, as shown in the insert keys. The NVT ensemble was applied throughout.

S6 NPT ensemble equilibration of aqueous acetic acid

Due to the absence of experimental solvent densities of aqueous acetic acid, under the commercial operating temperature (473 K) and pressure (2.25 MPa), NPT ensemble first principles MD simulations were performed to determine the unit cell density in order to run the subsequent NVT ensemble simulations.[14]

To ensure the choice of methodology was appropriate for predicting the macroscopic properties of the solvent, NPT ensemble simulations were run on 100% water and 100% acetic acid. The systems were equilibrated using the Chenoweth *et al.* ReaxFF forcefield for 25 ps, then equilibrated using first principles MD.[15] The density of the unit cell as a function of simulation time is shown in Figure S15.

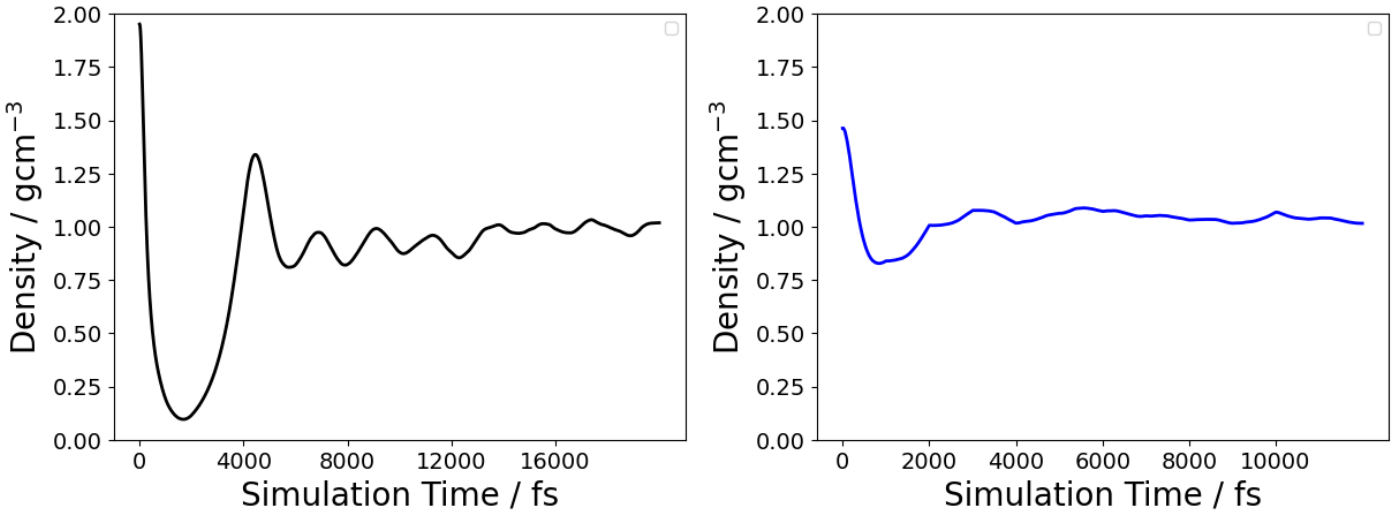

Fig. S15 Unit cell density for (left) water and (right) acetic acid at T = 298 K, p = 1 atm as a function of simulation time.

The equilibrated density for acetic acid was found to be 1.045 g/cm^3, with a standard deviation of 0.021 g/cm^3, as assessed from the final 10 ps of the simulation. The theoretical density was in much better agreement with the experimental density of 1.047 g/cm^3 than ReaxFF, and able to predict the physical macroscopic properties of the system. The equilibrated density for water was 0.946 g/cm^3, with a standard deviation of 0.06 g/cm^3, as assessed from the final 15 ps of the simulation. Similar to acetic acid, the first principles MD simulation agrees well with the experimental value of 1.0 g/cm^3, although under-predicts the density. Underestimation of the density of water by GGA functionals with dispersion schemes is attributed to an overestimization of liquid water polarizability.[16]

First principles MD NPT ensemble simulations were then run on 33.3 mol% aqueous acetic acid under a temperature of 473 K and pressure of 2.25 MPa. The equilibrated density of acetic acid was 0.894 $\pm$ 0.046 g/cm^3, as assessed from the final 27 ps of the simulation. Upon the introduction of 33.3 mol% water in the unit cell, the density decreased slightly to 0.885 $\pm$ 0.051 g/cm^3, as assessed from the final 22.5 ps of the simulation. The equilibrated density of 0.885 g/cm^3 was used for the reported NVT ensemble simulations.

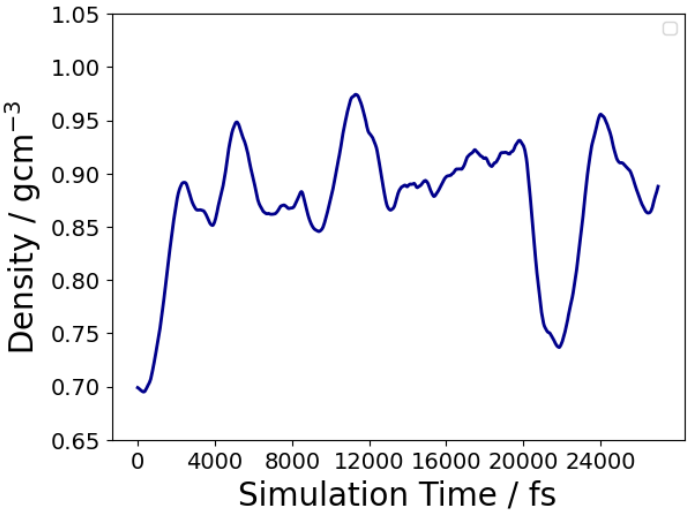

Fig. S16 Unit cell density for 33.3 mol% aqueous acetic acid under commercial operating conditions (T = 473 K, p = 2.25 MPa) as a function of simulation time.

S7 Size of simulation cell

Accurate simulation representation of experiment requires converged behaviour of the solvent environment. We have therefore considered the accuracy of our representation of the solvent system as a function of supercell size. Using the *NPT* calibrated unit cells determined in Section S6, *NVT* simulations have been performed with a 3 × 3 × 3 and a 4 × 4 × 4 supercell representation of the solvent system, *i.e.*, 27 and 64 solvent molecules, respectively. The benchmark calculations were performed for water under standard conditions; and for 33.3 mol% aqueous acetic acid under commercial operating conditions (Figure S17). The increased size of the 4 × 4 × 4 supercell impacts calculation speed, with the calculations on these systems more expensive than the 3 × 3 × 3 supercell by a factor of 2.4; therefore, the duration of the simulations used to construct the RDFs were restricted to 12 ps and 20 ps for the 100% water and 33.3 mol% aqueous acetic acid solvents, respectively.

The simulation results match for the different supercell sizes, showing the structural order is converged for the smaller cell. Furthermore, the position of the prominent peaks for the simulation of water under standard conditions align with the experimental RDF, with three peaks at approximately 2.8, 4.5 and 6.6 Å , respectively[17]. Given both 3 × 3 × 3 and 4 × 4 × 4 supercell sizes show converged behaviour of the solvent environment, and the 2.4× increase in the computational cost when increasing the size of the supercell from 27 to 64 solvent molecules, it can be concluded that a 3 × 3 × 3 supercell is appropriate for all further simulations.

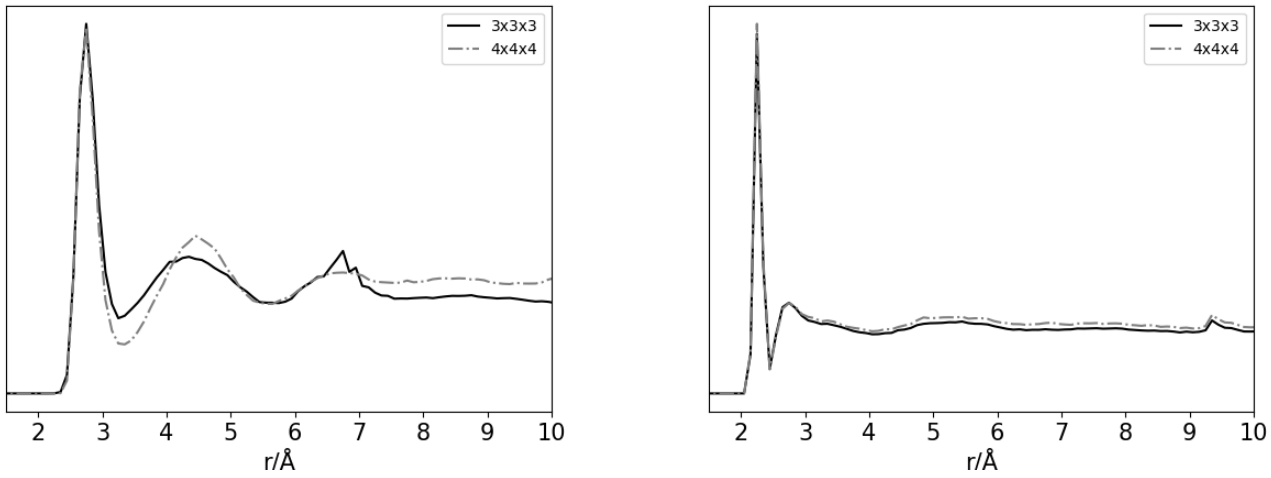

Fig. S17 O-O partial RDF for (left) water under standard conditions (T = 298 K, p = 0.1 MPa) and (right) 33.3 mol% aqueous acetic acid under commercial operating conditions (T = 473 K, p = 2.25 MPa). The RDF were calculated for every 5th structure during the simulation, using a bin width of 0.1 Å, then peak intensities were averaged over all considered images to obtain a statistically averaged RDF. Peak heights were normalized against the peak at 2.8 and 2.3 Å for the water and aqueous acetic acid RDF, respectively.

S8 Statistical analysis protocol used for analysis of the molecular dynamics simulations

For the molecular dynamics simulations, the chemical formula of the inner-sphere manganese complex, and the hapticity of the ligands was determined using a Python script.[18] To determine the ligands coordinating to manganese, a cutoff of 1.5× the covalent radii of each atomic species was used. This cutoff radii threshold was selected after extensive testing. In general, the testing showed smaller cutoff radii than 1.5× lead to some inner-sphere ligands not being captured and larger cutoff radii lead to outer-sphere solvent molecules being captured.

Chemical formulas of the inner-sphere manganese complexes was determined for all structures present in the MD simulations. These were then counted to determine the percentage ratio of each complex throughout the simulation. For some of the identified chemical formulas, the choice of cutoff radius meant outer-sphere ligands were included in the chemical formula. Therefore these structures were manually checked, with 90 % of the total structures being included in the reported statistics. This threshold (90 %) was chosen as it was not feasible to manually check all structures.

Reported residence times for water and acetic acid were calculated as the average time a water or acetic acid molecule was present in the inner solvation sphere of the manganese cation before leaving to the outer-sphere.

S9 Further details of the complexes observed during the molecular dynamics simulations

S9.1 Changes in Coordination Number

Figure S18 shows the coordination number of the Mn(II) and Mn(III) complexes with and without HBr as a function of the simulation time. For Mn(II) in 33.3 mol% aqueous acetic acid, 3-, 4-, 5-, 6-, and 7-coordinate structures are observed; whereas for Mn(III) in 33.3 mol% aqueous acetic acid, 4-, 5-, 6-, and 7-coordinate structures are observed. The 5- and 6- coordinate species are non-transient and exist on a picosecond timescale; whereas the 3-, 4- and 7- coordinate species are identified as transient as they only last for short periods only (less than a few hundred femtoseconds at most). For Mn(III) in the presence of HBr, no 7-coordinate complexes are observed, and the complexes present are 4-, 5-, and 6- coordinate.

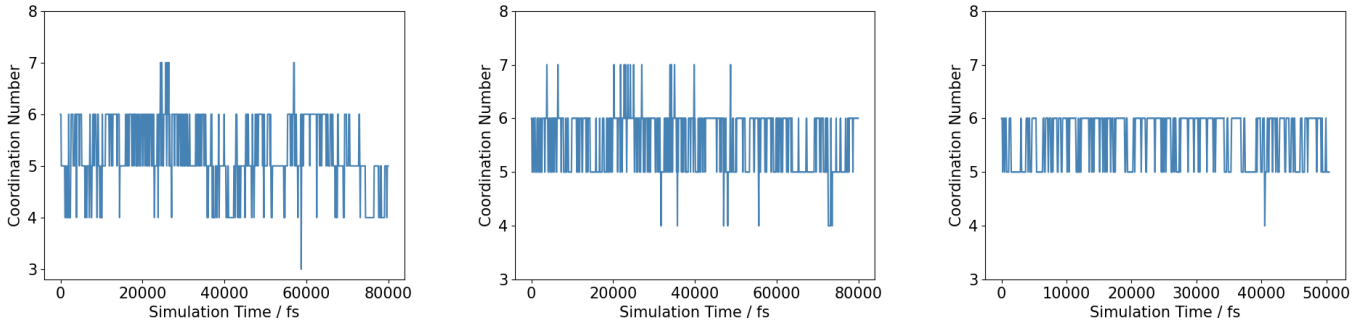

Fig. S18 Graphs of the coordination number of the analyzed manganese complexes during the MD simulations in 33.3 mol% aqueous acetic acid, plotted against simulation time. Left: Mn(II) without HBr; Middle: Mn(III) without HBr; Right: Mn(III) with HBr. An interval of 100 fs has been used for plotting.

S9.2 Full statistical analysis of the observed complexes

Figures S19 – S22 show the analyses of all the coordination environments observed during the first principles molecular dynamics simulations. For Mn(II), the coordination number is observed as predominantly five coordinate, with the 5- and 6- coordinate species constituting 48.1% and 36.2% of the total observed complexes, respectively; 4-coordinate structures were observed for 14.5% of the simulation time, and 7-coordinate structures for 1.1% of the simulation. The Mn(III) complexes in 33.3 mol% aqueous acetic acid exist predominantly as a six coordinate species, with 40.8% and 55.8% of structures observed to be 5- and 6- coordinate, respectively; only 1.6% are 4-coordinate, and 1.8% are 7-coordinate. The most common coordination is similar when a HBr moiety is included in the supercell, with 35.6% and 64.1% of complexes observed to be 5- and 6- coordinate, respectively; whilst 4-coordinate structures constitute only 0.3% of the observed structures. The greater proportion of 6-coordinate structures in the simulations with Mn(III) than those with Mn(II) can be attributed to the stronger electrostatic interaction when the cation charge increases from Mn(II) to Mn(III), meaning the ligands bind more strongly, and closely, to the metal center.

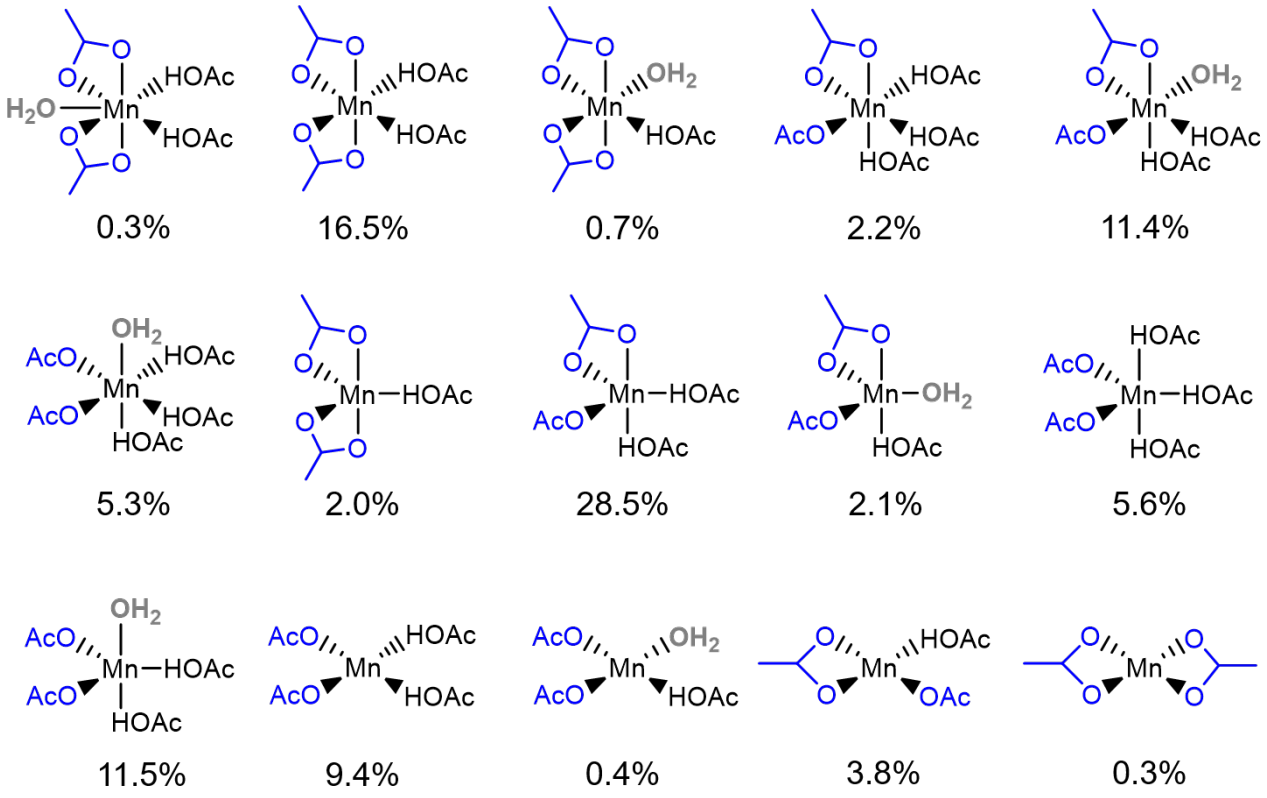

Fig. S19 Statistical analysis of all structures observed in the 80 ps first principles MD simulation of Mn(II) species in 33.3 mol% aqueous acetic acid. The total time water and acetic acid are in the inner coordination sphere are 25.4 ps and 79.8 ps, respectively.

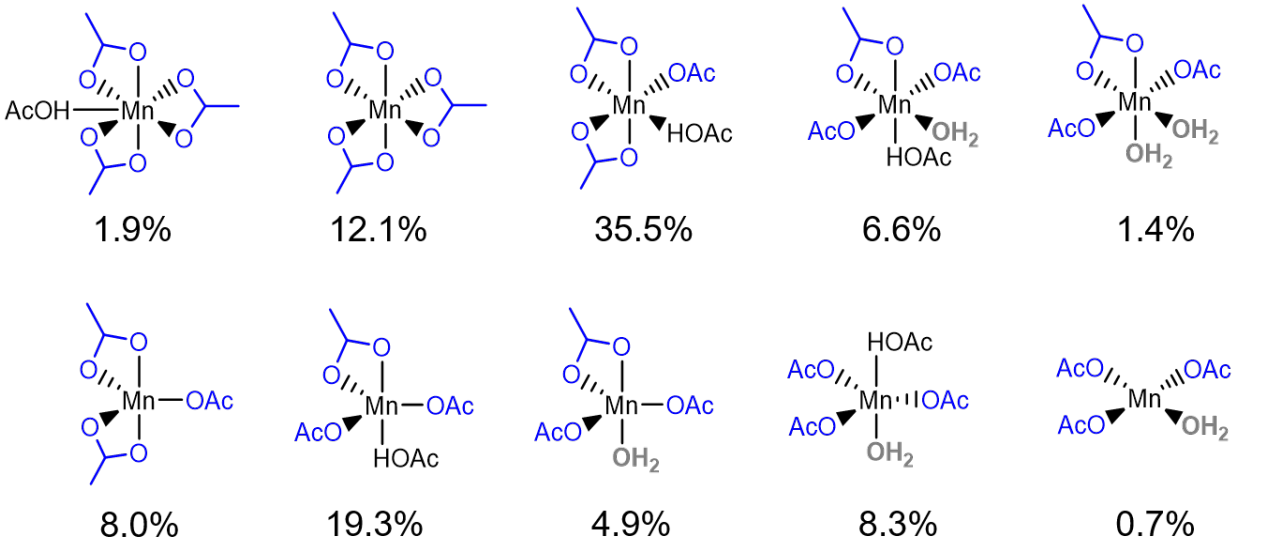

Fig. S20 Statistical analysis of all structures observed in the 80 ps first principles MD simulation of Mn(III) species in 33.3 mol% aqueous acetic acid. The remaining 1.3% of structures not shown correspond to hydroxylated structures where an inner-sphere water was deprotonated by a ligand in the outer-sphere; these hydroxylated structures were observed to have one coordinating water. The total time water and acetic acid are in the inner coordination sphere is 17.5 ps and 57.3 ps, respectively.

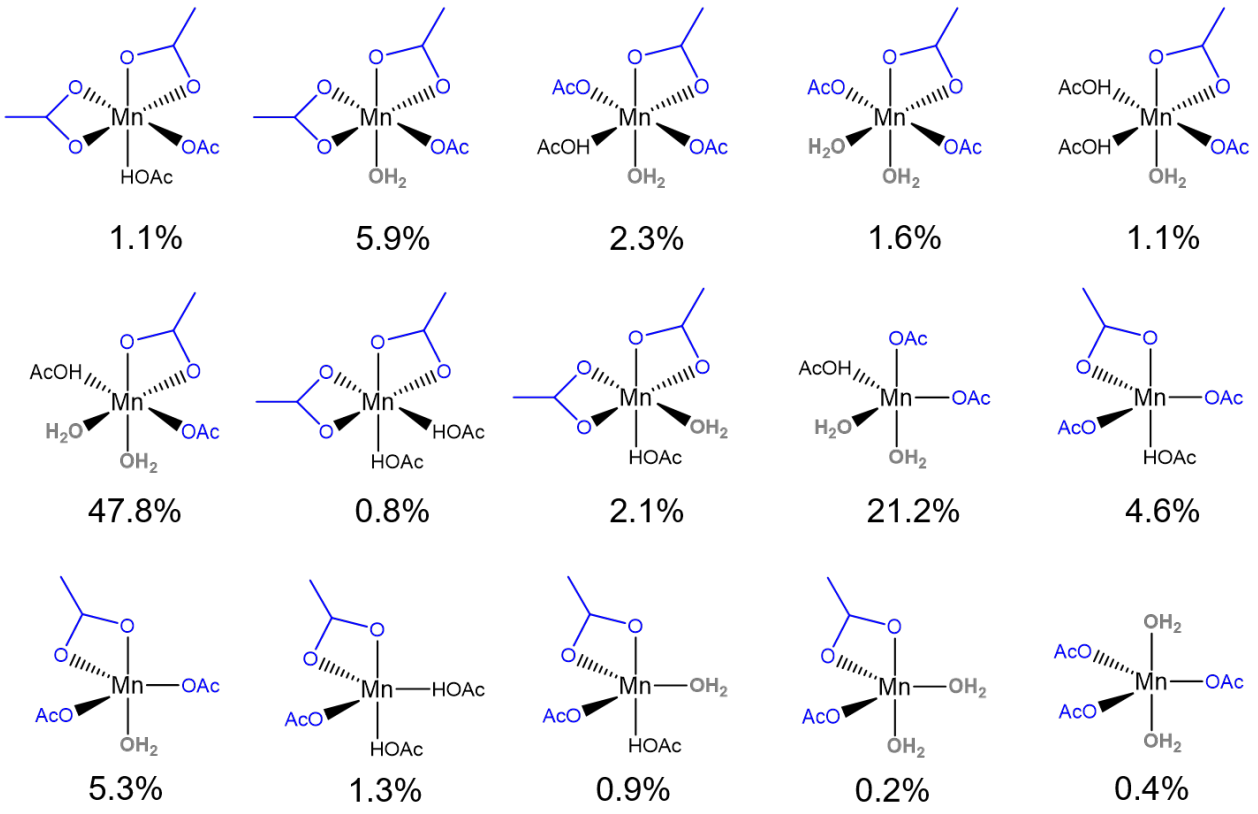

Fig. S21 Statistical analysis of the structures observed in the 50 ps production MD simulation of Mn(III) species in 33.3 mol% aqueous acetic acid and a HBr moiety. The remaining 3.4% of structures not shown correspond to hydroxylated structures where an inner-sphere water was deprotonated by a ligand in the outer-sphere; of these hydroxylated structures, 3.3% were observed to have one coordinating water and 0.1% zero coordinating water. The total time water and acetic acid are in the inner coordination sphere is 44.4 ps and 41.6 ps, respectively.

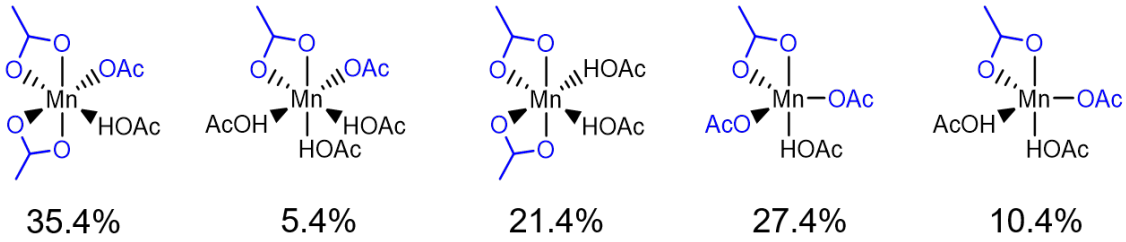

Fig. S22 Statistical analysis of the structures observed in the 50 ps production MD simulation of Mn(III) species in 33.3 mol% aqueous acetic acid and a H^+ moeity. The total time water and acetic acid are in the inner coordination sphere is 0 ps and 80 ps, respectively.

Notes and references

1 H. Ohtaki and T. Radnai, *Chemical Reviews*, 1993, **93**, 1157–1204.

2 I. Persson, *Pure and Applied Chemistry*, 2010, **82**, 1901–1917.

3 J. P. Perdew, K. Burke and M. Ernzerhof, *Physical Review Letters*, 1996, **77**, 3865.

4 C. Adamo and V. Barone, *The Journal of Chemical Physics*, 1999, **110**, 6158–6170.

5 Y. Zhao and D. G. Truhlar, *Theoretical Chemistry Accounts*, 2008, **120**, 215–241.

6 V. Blum, R. Gehrke, F. Hanke, P. Havu, V. Havu, X. Ren, K. Reuter and M. Scheffler, *Computer Physics Communications*, 2009, **180**, 2175–2196.

7 A. Tkatchenko and M. Scheffler, *Physical Review Letters*, 2009, **102**, 073005.

8 A. Tkatchenko, R. A. DiStasio Jr, R. Car and M. Scheffler, *Physical Review Letters*, 2012, **108**, 236402.

9 A. Tkatchenko, A. Ambrosetti and R. A. DiStasio Jr, *The Journal of Chemical Physics*, 2013, **138**, 074106.

10 C. J. Cramer and D. G. Truhlar, *Free Energy Calculations in Rational Drug Design*, 2001, 63–95.

11 C. J. Cramer and D. G. Truhlar, *Trends and Perspectives in Modern Computational Science*, 2006, **6**, 112–140.

12 R. L. Taylor, D. Housley, M. Barter, A. Porch, K. Whiston, A. Folli and D. M. Murphy, *Catalysis Science & Technology*, 2022, **12**, 5274–5280.

13 T. Sun, D. Ly and A. S. Teja, *Industrial & Engineering Chemistry Research*, 1995, **34**, 1327–1331.

14 M. Li, F. Niu, D. H. Busch and B. Subramaniam, *Industrial & Engineering Chemistry Research*, 2014, **53**, 9017–9026.

15 K. Chenoweth, A. C. Van Duin and W. A. Goddard, *The Journal of Physical Chemistry A*, 2008, **112**, 1040–1053.

16 S. Y. Willow, X. C. Zeng, S. S. Xantheas, K. S. Kim and S. Hirata, *The Journal of Physical Chemistry Letters*, 2016, **7**, 680–684.

17 D. H. Brookes and T. Head-Gordon, *The Journal of Physical Chemistry Letters*, 2015, **6**, 2938–2943.

18 *CARMM repository*, 2024, `https://github.com/logsdail/carmm/`.